Chemical pressure effects on structural, magnetic, and transport properties of $Mn_{1-x}Co_xV_2O_4$

A. Kiswandhi,[1,2] J. S. Brooks,[1,2] J. Lu,[1] J. Whalen,[1] T. Siegrist,[1,3] and H. D. Zhou[1,*]

[1]*National High Magnetic Field Laboratory, Florida State University, Tallahassee, Florida 32306-4005, USA*

[2]*Department of Physics, Florida State University, Tallahassee, Florida 32306-3016, USA*

[3]*Department of Chemical and Biomedical Engineering, Florida State University, Tallahassee, Florida 32310, USA*

(Received 5 October 2011; revised manuscript received 14 November 2011; published 29 November 2011)

We present the low-temperature XRD, susceptibility, specific heat, and resistivity results on single crystal $Mn_{1-x}Co_xV_2O_4$. With increasing Co doping, the chemical pressure related to the decreasing V-V distance drives the system toward the itinerant electron limit, accompanied with the increase of the ferrimagnetic transition temperature and the suppression of the structural distortion. These effects are compared to pressure effects, and show that the V-V distance is the critical parameter controlling the properties of AV_2O_4.

DOI: 10.1103/PhysRevB.84.205138 PACS number(s): 72.80.Ga, 71.30.+h, 75.50.Dd, 61.05.cp

I. INTRODUCTION

Normal spinels[1] AV_2O_4 (A = Cd, Mn, Fe, Mg, Zn, and Co) with fixed valence of V^{3+} ions has been a hot topic due to their two abnormal physical properties: (i) the orbital ordering transition that originates from the localized V^{3+} ($3d^2$) electrons with t_{2g} orbital freedom, positioned on a geometrically frustrated pyrochlore-like structure. This orbital ordering transition usually drives a cubic to tetragonal structural phase transition at low temperatures, such as for CdV_2O_4,[2–4] MnV_2O_4,[5–9] FeV_2O_4,[10,11] MgV_2O_4,[12,13] and ZnV_2O_4.[4,14,15] (ii) the approach to the itinerant electron limit with decreasing V-V separation ($R_{V\text{-}V}$).[16,17] The predicted critical V-V separation for the metallic behavior is $R_c = 2.94$ Å.[18] Several studies have supported this prediction. For example, the pressure studies on magnetization of AV_2O_4 have shown that the passage from the localized to itinerant electron limit occurs through an intermediate phase, in which the sample shows large pressure dependence of magnetic transition temperature due to the electronic delocalization in cation clusters. ZnV_2O_4 and MgV_2O_4 with small $R_{V\text{-}V}$ may be situated in this intermediate phase.[19] Furthermore, the theoretical calculations show that in ZnV_2O_4 partial electron delocalization, not orbital ordering, leads to a structural instability to form V-V dimers.[20]

Recently our studies on CoV_2O_4[21] show that the metallic behavior can be induced under high pressure, which is strong evidence for the existence of R_c. These pressure studies on AV_2O_4 clearly show that high pressure can change the properties significantly by reducing the lattice size and V-V distance. Another efficient way to vary the V-V distance is to apply chemical pressure. In this paper we present the low-temperature x-ray diffraction (XRD), susceptibility, specific heat, and resistivity results on single crystal $Mn_{1-x}Co_xV_2O_4$. We study how the chemical pressure imposed by the Co doping affects the structural, magnetic, and transport properties of $Mn_{1-x}Co_xV_2O_4$ by changing the V-V distance. We also compare the chemical pressure effects to those of physical pressure.

II. EXPERIMENT

Single crystals of $Mn_{1-x}Co_xV_2O_4$ were grown by the traveling-solvent floating-zone (TSFZ) technique. The feed and seed rods for the crystal growth were prepared by solid state reaction. Appropriate mixtures of MnO, CoO, and V_2O_3 were ground together and pressed into 6-mm-diameter 60-mm rods under 400 atm hydrostatic pressure, and then calcined in vacuum in a sealed quartz tube at 950 °C for 12 h. The crystal growth was carried out in argon in an IR-heated image furnace (NEC) equipped with two halogen lamps and double ellipsoidal mirrors with feed and seed rods rotating in opposite directions at 25 rpm during crystal growth at a rate of 30 mm/h. Due to the evaporation of V_2O_3 during the growth, extra V_2O_3 in the starting material and high growth speeds are critical to obtain high quality samples. Small pieces of single crystals were ground into fine powder for XRD, and the diffraction patterns were recorded with a HUBER Imaging Plate Guinier Camera 670 with Ge monochromatized Cu $K_{\alpha 1}$ radiation (1.54059 Å). Data were collected at temperature down to 10 K with a cryogenic helium compressor unit. The lattice parameters were refined from the XRD patterns by using the program WINPREP[22] with typical $0.02 \leqslant R_w \leqslant 0.03$ residuals. X-ray Laue diffraction was used to confirm crystal quality. The dc magnetic-susceptibility measurements were performed using a Quantum Design superconducting interference device (SQUID) magnetometer. The specific heat measurements were performed on a Quantum Design physical property measurement system (PPMS). The resistivity was measured with a four probe technique. The pressure was applied on a sample with $x = 0.7$ by using Daphne oil 7373 as a pressure medium in a standard piston cylinder clamp cell.

III. RESULTS

A. X-ray diffraction

Lattice parameters obtained from the room temperature powder XRD for the cubic $Fd\bar{3}m$ spinel system $Mn_{1-x}Co_xV_2O_4$ indicate a complete solid solution over the range ($0 \leqslant x \leqslant 1.0$). In accordance with Végard's law, the lattice parameter a decreases linearly with increasing x (Fig. 1). The $R_{V\text{-}V}$ is calculated and is shown as $1/R_{V\text{-}V}$ vs x in Fig. 1. With increasing Co doping x, $R_{V\text{-}V}$ decreases as the chemical pressure increases. To show the effects of chemical pressure, the physical properties of $Mn_{1-x}Co_xV_2O_4$ listed below are plotted as a function of $1/R_{V\text{-}V}$ instead of x.

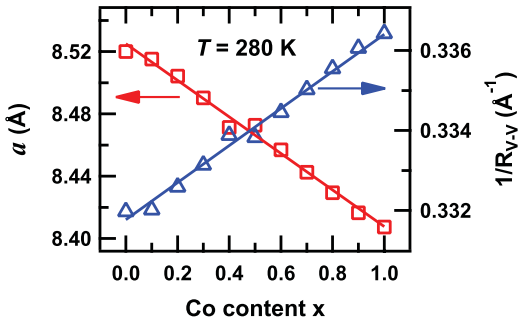

FIG. 1. (Color online) Variation with x of the lattice parameter a and $1/R_{\text{V-V}}$ for $Mn_{1-x}Co_xV_2O_4$.

Low-temperature XRD experiments were done to investigate the structural phase transition in single crystal $Mn_{1-x}Co_xV_2O_4$. For low Co-doping samples with $0.1 \leqslant x \leqslant 0.7$, the structure changes from cubic to tetragonal $I4_1/amd$ symmetry at low temperatures, which is similar to pure MnV_2O_4. As shown in Fig. 2(b), the XRD pattern at $T = 10$ K of $x = 0.3$ sample clearly shows peak splitting from the room temperature XRD pattern [Fig. 2(a)] due to the structural phase transition. On the other hand, for high Co-doping samples with $0.8 \leqslant x < 1.0$, the cubic structure remains unchanged down to 10 K, which is similar to the pure CoV_2O_4 without a structural phase transition. As shown in Figs. 2(c) and 2(d), the XRD pattern at $T = 10$ K of $x = 0.8$ sample shows no difference from the room temperature pattern besides the shift due to the lattice contraction with decreasing temperature. The detailed low temperature XRD measurements (1 K/step) in the proximity of the transition have been performed to find the structural phase transition temperature for each sample. Figure 3 shows the temperature dependence of the lattice parameters for $0.1 \leqslant x \leqslant 0.8$ samples. For $0.1 \leqslant x \leqslant 0.7$, one general trend is that the structural phase transition temperature (T_s) decreases with increasing Co

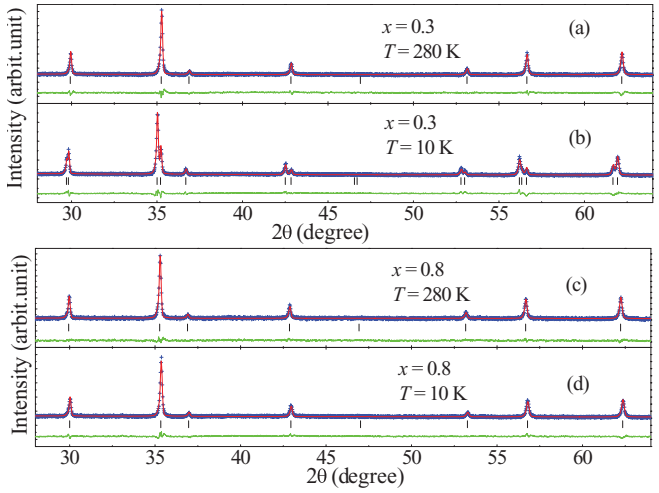

FIG. 2. (Color online) XRD patterns (crosses) for $x = 0.3$ sample at (a) 280 K and (b) 10 K, and for $x = 0.8$ sample at (c) 280 K and (d) 10 K. The solid curves are the best fits from the Rietveld refinement using FULLPROF. The vertical marks indicate the position of Bragg peaks and the bottom curves show the difference between the observed and calculated intensities.

doping. It is clear that for $x = 0.8$ there is no structural change above 10 K.

The c/a ratio in the tetragonal phase increases with increasing Co doping. Here the a is calculated as $\sqrt{2}a_t$ and a_t is the lattice parameter for the tetragonal phase for comparison to the lattice parameter a in the cubic phase. The large c/a ratio means a small difference between c and a lattice parameters, indicating a weak structural distortion. For $x \geqslant 0.8$ samples without structural change, $c/a = 1$. In order to show this trend more clearly, we plotted the temperature dependence of the (400) peak for $x = 0.1$, 0.5, 0.7, and 0.8 in Fig. 4, where, with decreasing temperature, the (400) peak splits to (400) and (004) peaks below T_s. For $x = 0.8$, the (400) peak does not split above 10 K. It is clear that the splitting between the (400) and (004) peaks decreases with increasing Co doping, indicating a weaker structural distortion in the tetragonal phase or an increase of c/a ratio. The c/a ratio at 10 K for $Mn_{1-x}Co_xV_2O_4$ is shown in Fig. 5.

B. Susceptibility and specific heat

Figure 6 shows the temperature dependence of magnetic susceptibility and specific heat for $Mn_{1-x}Co_xV_2O_4$. For $x = 0.1$, 0.2, 0.3, and 0.4, the specific heat data shows two peaks. The high temperature peak occurs at the same temperature where the susceptibility shows a sharp increase. Therefore, this peak represents the ferrimagnetic transition (T_C) for $Mn_{1-x}Co_xV_2O_4$, where the Mn(Co) spins and V spins align in the opposite direction. The low temperature peak is a very sharp peak for these four samples and occurs at the same temperature where the zero field cooling susceptibility (ZFC) shows a sharp drop; this temperature is also where the structural phase transition observed from the low temperature XRD measurements occurs. Therefore, this sharp peak represents the structural phase transition (T_S). The divergence between the ZFC and field cooling (FC) susceptibility at T_S is a sign for a glassy magnetic state, or perhaps a cluster spin glass, which is also revealed by the frequency dependence of the ac susceptibility from Ref. 7. For $x = 0.5$, 0.6, and 0.7, the specific heat still shows the high temperature peak. But the low temperature sharp peak becomes very weak, which is shown as a broad peak instead. Accordingly, the sharp drop from ZFC susceptibility data for these three samples are not observable anymore. For $x = 0.8$, 0.9, and 1.0, the specific heat just shows one peak around T_C and the low temperature peak disappears above 2 K. The behavior of the peak around T_S shown from specific heat is consistent with the XRD results: the structural distortion becomes weak with increasing Co doping and disappears for $x \geqslant 0.8$.

It should be noted that for MnV_2O_4 (i.e., $x = 0$ in Fig. 6) the sharp peak occurs at higher temperature (56 K) than the other peak (53 K). Our previously detailed studies show this sharp peak is actually related to T_C, and the lower temperature peak is related to T_S.[23] Although other reports for $x = 0$ ascribe the higher temperature peak to T_S and the lower temperature peak to T_C,[7] our studies for $Mn_{1-x}Co_xV_2O_4$ unambiguously show that T_C, which is coincident with rapid rise in the susceptibility, is always higher than T_S for Co-doped samples, and T_C increases and T_S decreases with increasing Co doping.

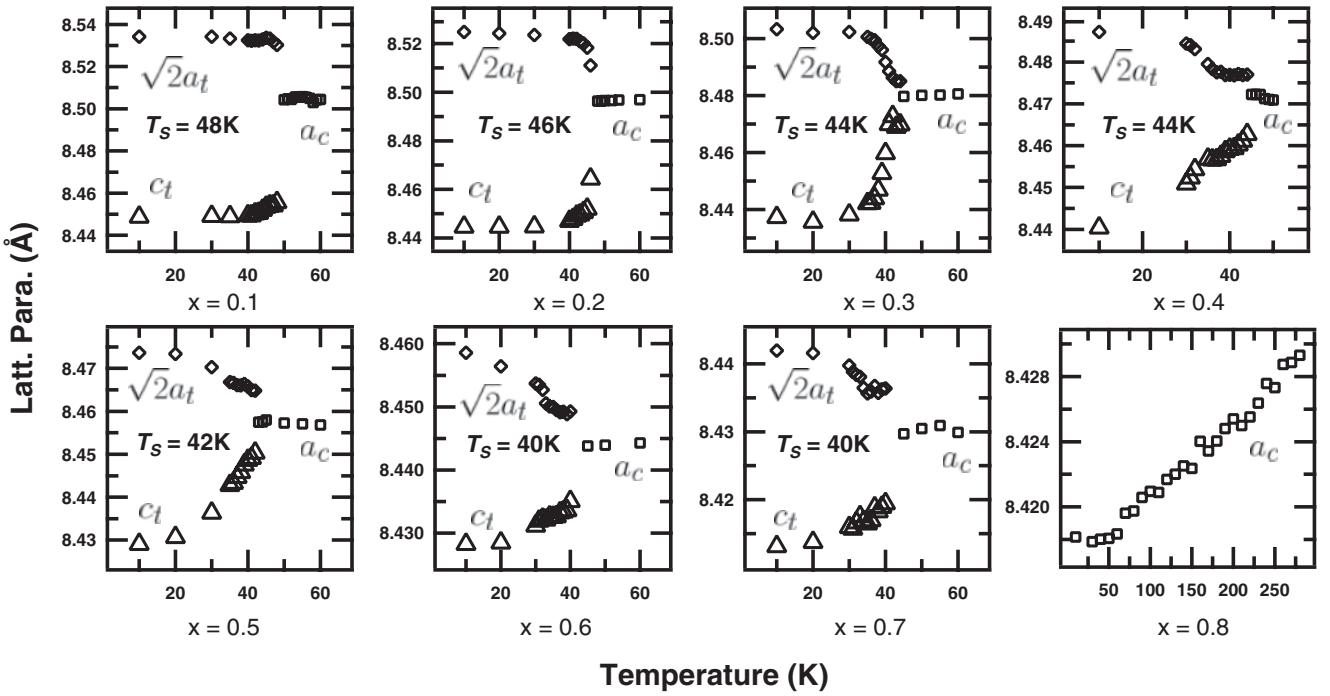

FIG. 3. The temperature dependences of the lattice parameters for $0.1 \leqslant x \leqslant 0.8$ samples.

C. Resistivity

For all $Mn_{1-x}Co_xV_2O_4$ $(0 \leqslant x \leqslant 1.0)$ samples, the resistivity shows semiconducting behavior below room temperature, as shown in Fig. 7(a). With increasing chemical pressure (or $1/R_{V\text{-}V}$), the resistivity decreases significantly. For example, at room temperature, the resistivity for MnV_2O_4 is around 1000 Ω cm, and for CoV_2O_4 the resistivity decreases to around 0.1 Ω cm, as plotted in Fig. 8(a). For $x \geqslant 0.4$

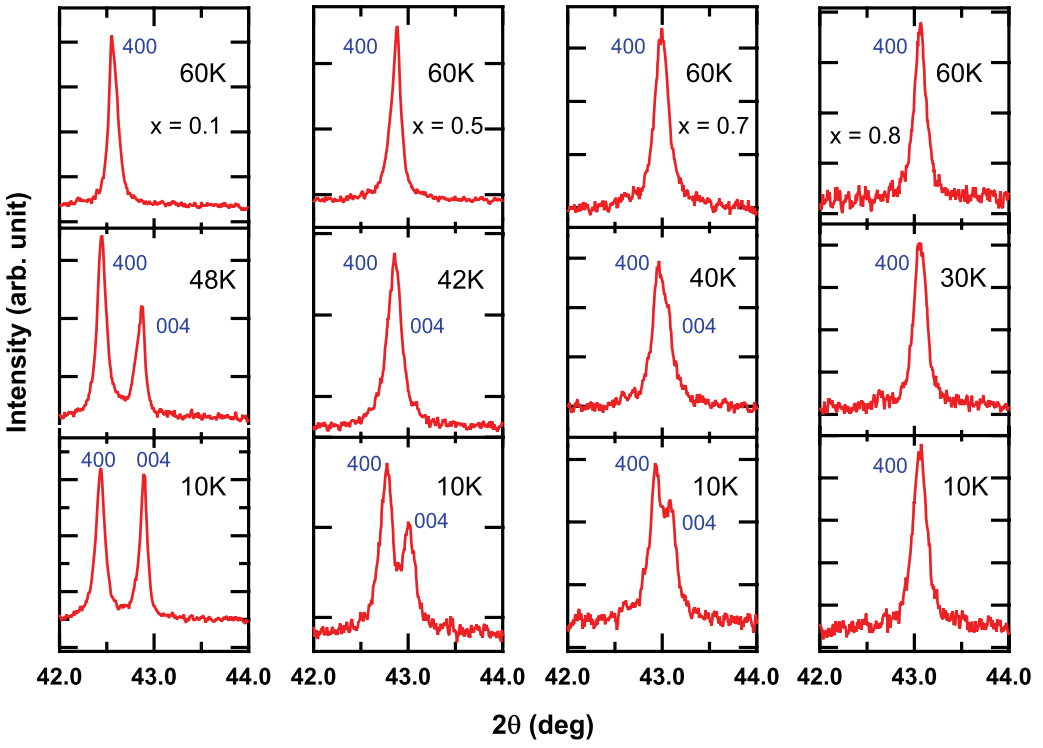

FIG. 4. (Color online) The temperature dependence of (400) peak splitting for $x = 0.1$, 0.5, 0.7, and 0.8 samples.

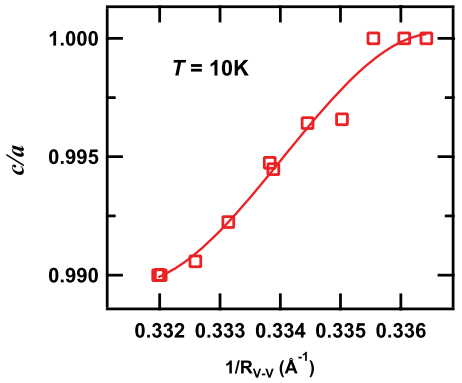

FIG. 5. (Color online) Variation with $1/R_{\text{V-V}}$ of the c/a ratio for $Mn_{1-x}Co_xV_2O_4$.

samples, the resistivity shows a λ-type anomaly around T_C. For these samples, T_C is also determined as the dip position of $d\ln\rho/dT^{-1}$ vs T curves [Fig. 8(b)]. T_C increases with increasing Co doping. Above T_C, the behavior of the resistivity of $Mn_{1-x}Co_xV_2O_4$ can be divided to two different types: (i) For $0 \leqslant x \leqslant 0.7$, a good fit is achieved with $\rho \propto \exp[(T_0/T)^{1/4}]$, the Mott variable-range hopping (VRH) model,[24] as shown in Fig. 7(c). With increasing chemical pressure, T_0 decreases [Fig. 9(a)] significantly. (ii) For $x \geqslant 0.8$, the resistivity above

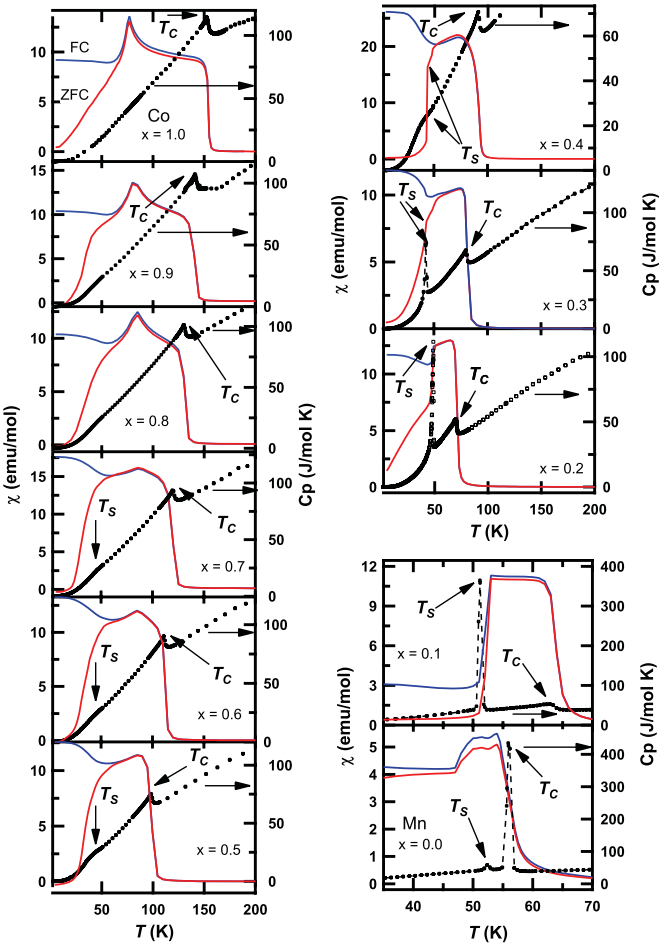

FIG. 6. (Color online) The temperature dependences of dc magnetic susceptibility and specific heat for $Mn_{1-x}Co_xV_2O_4$.

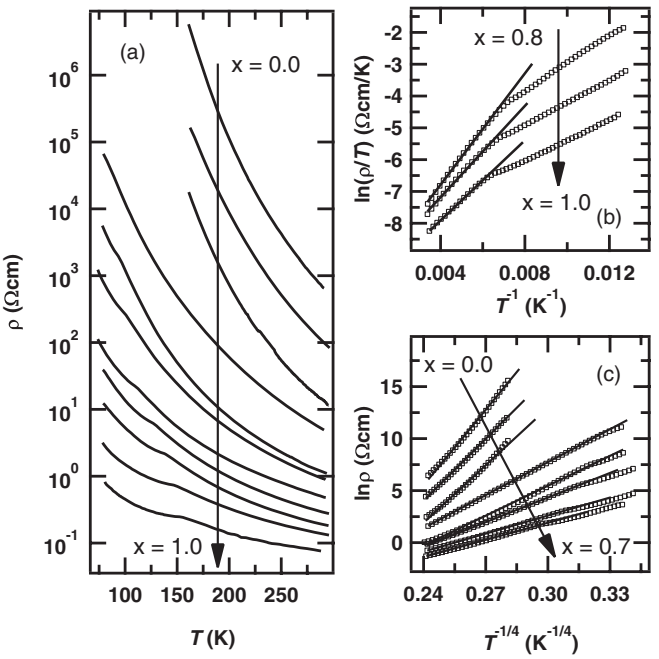

FIG. 7. (a) The temperature dependences of resistivity for $Mn_{1-x}Co_xV_2O_4$; (b) $\ln(\rho/T)$ vs T^{-1} curves for $x \geqslant 0.8$; and (c) $\ln(\rho)$ vs $T^{-1/4}$ curves for $0.1 \leqslant x \leqslant 0.7$ samples. The solid lines in (b) and (c) are linear fits as described in the text.

T_C can be well fitted by $\rho = \rho_0 T \exp(E_P/k_B T)$ for nearest-neighbor hopping of polarons [Fig. 7(b)]. E_P decreases with increasing chemical pressure [Fig. 9(b)].

The resistivity measured under different pressures for $Mn_{0.3}Co_{0.7}V_2O_4$ is shown in Fig. 10. With increasing pressure, the resistivity decreases. Here the T_C is again determined as the dip position of $d\ln(R/R_{RT})/dT^{-1}$ vs T curves [Fig. 11(a)] and T_C increases with increasing pressure [Fig. 11(b)]. The resistivity above T_C is well fit to the VRH model and the fitting parameter T_0 decreases with increasing pressure [Fig. 11(b)].

IV. DISCUSSION

With increasing Co doping, the chemical pressure increases with decreasing $R_{\text{V-V}}$, and the $Mn_{1-x}Co_xV_2O_4$ system approaches itinerant electron behavior as shown by the decreasing resistivity with decreasing V-V distance. This effect is consistent with previous studies on semiconducting AV_2O_4, where with decreasing V-V separation, AV_2O_4 approaches the itinerant-electron limit, and shows abnormal properties. For example, the study of the magnetic interactions under pressure for MnV_2O_4 shows a large pressure dependence of T_C. This is due to an anomalous compressibility near T_C as predicted for a double-well potential at the crossover from a longer to a shorter equilibrium V-V bond when the system is approaching the itinerant electron behavior.[19] This double-well potential can perturb the periodic potential, trapping the charge carriers, and give rise to VRH transport behavior at low Co doping ($0 < x \leqslant 0.7$). For the VRH model, $T_0 \propto \alpha^3/[k_B N(E_F)]$, where α^{-1} is the localization length, k_B is the Boltzmann constant, and $N(E_F)$ is the density of localized states at Fermi level. It is unlikely that the change of $N(E_F)$ with

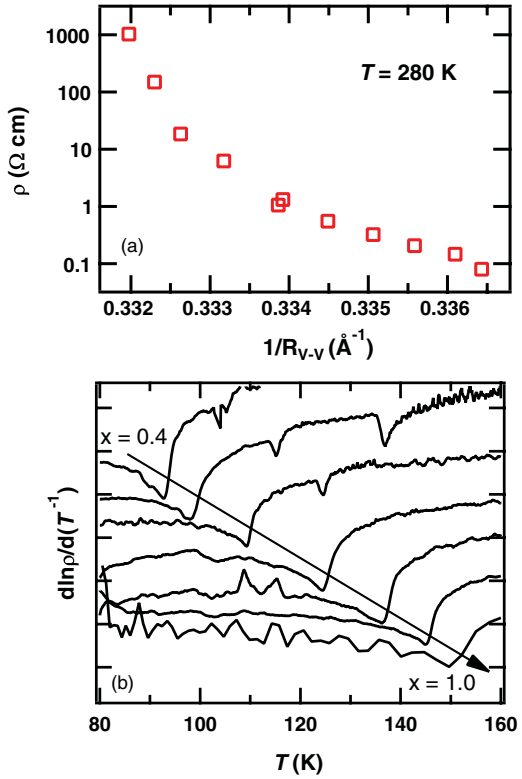

FIG. 8. (Color online) (a) Variation with $1/R_{\text{V-V}}$ of the room temperature resistivity for $Mn_{1-x}Co_xV_2O_4$. (b) The $d\ln(\rho)/dT^{-1}$ vs T curves for $x \geqslant 0.4$ samples.

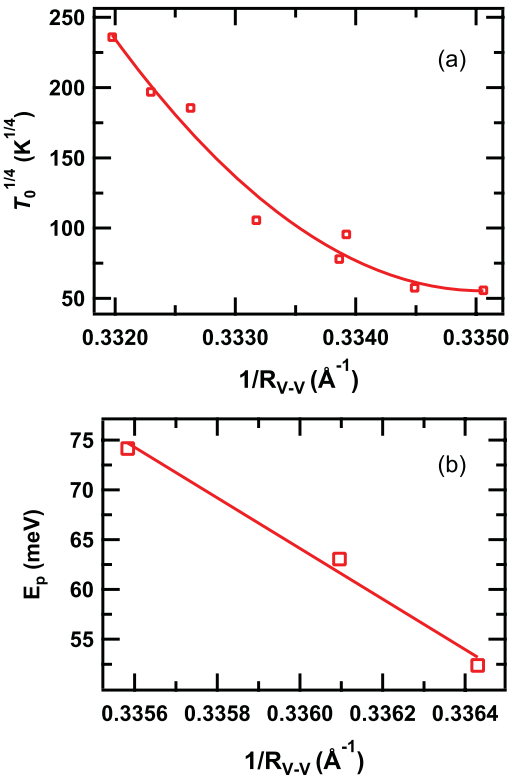

FIG. 9. (Color online) Variation with $1/R_{\text{V-V}}$ of the (a) $T_0^{1/4}$ and (b) E_P for $Mn_{1-x}Co_xV_2O_4$.

increasing chemical pressure for $Mn_{1-x}Co_xV_2O_4$ can account for the large decrease of T_0. Hence the decrease of T_0 implies the increase of localization length α^{-1}, leading to electronic delocalization. As the $Mn_{1-x}Co_xV_2O_4$ system approaches the itinerant electron limit by increasing chemical pressure for $x \geqslant 0.8$, the resistivity becomes smaller and is dominated by the formation of magnetic polarons. This behavior also has been found in other ferrimagnetic spinels, for example, $FeCr_2S_4$.[25–27]

We have also compared the effects from chemical pressure and physical pressure on the $Mn_{1-x}Co_xV_2O_4$ system. The resistivity under pressure for a $x = 0.7$ sample shows that the resistivity and T_0 both decrease with increasing pressure, which means electronic delocalization under pressure. This effect is the same as the chemical pressure as we mentioned above. Our previous study on pure CoV_2O_4, which has the smallest V-V distance,[21] showed that the pressure could induce metallic behavior. If we assume the $x = 0.7$ sample and CoV_2O_4 have the same compressibility as that of MnV_2O_4,[19] we then can calculate the pressure-induced variation of T_C with $1/R_{\text{V-V}}$ for $Mn_{1-x}Co_xV_2O_4$. As shown in Fig. 12, the increase of T_C induced by the chemical pressure (open symbols) and physical pressure (the crosses) show similar linear dependence on $1/R_{\text{V-V}}$. This confirms that the chemical and physical pressure effects on T_C are similar. For a magnetic insulator, the magnetic transition temperature T_C is proportional to the spin-spin superexchange interaction $T_C \sim J \sim t^2/U$.[28] Here t is the charge transfer between sites and U is the intra-atomic Coulomb energy. Since t is proportional to the overlap integral for the donor and acceptor orbitals on neighboring atoms, t is also a function of the interionic distance R. Normally, the shorter distance of R leads to stronger t. For $Mn(Co)V_2O_4$, due to the t^2e^0 configuration of the V^{3+} ion, the V-V interaction across the shared octahedral-site edges is the strong interaction relative to the Mn(Co)-O-V interactions.[29] Therefore, for $Mn(Co)V_2O_4$, t could be simplified to be a function of the V-V distance. With increasing chemical (or physical) pressure, if we assume that U remains constant, the decreasing V-V distance of $Mn(Co)V_2O_4$ will lead to a monotonic increase of t or J or T_C. The T_C with $1/R_{\text{V-V}} > 0.338$ Å^{-1} is calculated from the resistivity data under pressure larger than 2 GPa for CoV_2O_4. Under this pressure, CoV_2O_4 is approaching the itinerant electron limit and the assumption that U remains constant breaks down, which may lead, in our estimate, to the deviation from linear behavior for the $1/R_{\text{V-V}}$ dependence of T_C.

The increasing chemical pressure in $Mn_{1-x}Co_xV_2O_4$ also leads to the decrease of T_s and finally the disappearance of the structural distortion for $x \geqslant 0.8$ samples. This is consistent with the fact that the system is approaching the itinerant electron limit with the increasing chemical pressure. For $0 \leqslant x \leqslant 0.7$, the system is still dominated by the localized electron behavior. The cubic to tetragonal structure transition is due to the orbital ordering of V^{3+} ($3d^2$) electrons with t_{2g} orbitals, as in other insulating AV_2O_4 spinels. For shorter V-V distances approaching the itinerant electron limit, the weaker structural distortion or structural instability has been theoretically argued to be due to the formation of homopolar V-V covalent bonds from the partial electronic delocalization, and not orbital ordering.[20] Therefore, for $x \geqslant 0.8$ samples,

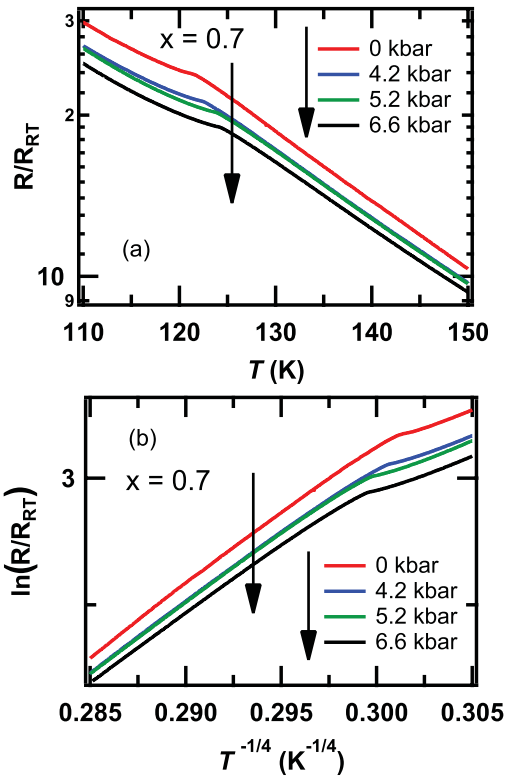

FIG. 10. (Color online) (a) The temperature dependencies of R/R_{RT} under different pressures for $Mn_{0.3}Co_{0.7}V_2O_4$; (b) $\ln(R/R_{RT})$ vs $T^{-1/4}$ curves under different pressures for $Mn_{0.3}Co_{0.7}V_2O_4$. R_{RT} is the resistance at room temperature.

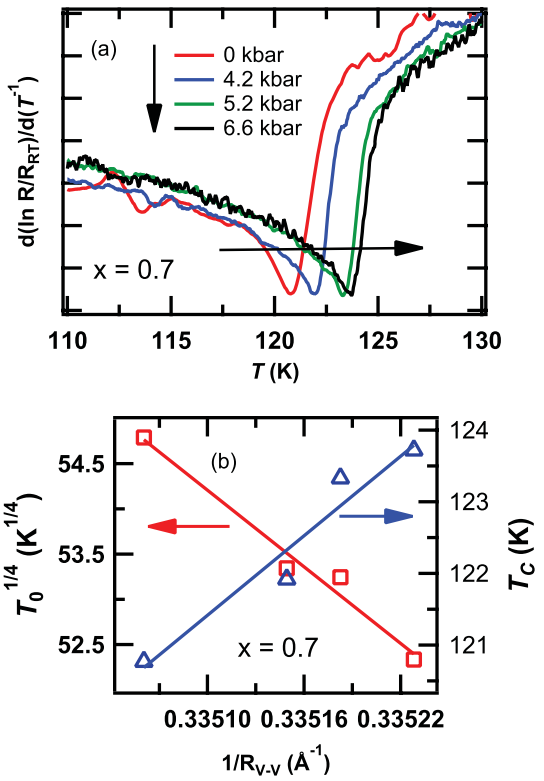

FIG. 11. (Color online) (a) The $d\ln(R/R_{RT})/dT^{-1}$ vs T curves under different pressures for $Mn_{0.3}Co_{0.7}V_2O_4$ and (b) variation with $1/R_{V\text{-}V}$ of T_C and $T_0^{1/4}$ for $Mn_{0.3}Co_{0.7}V_2O_4$.

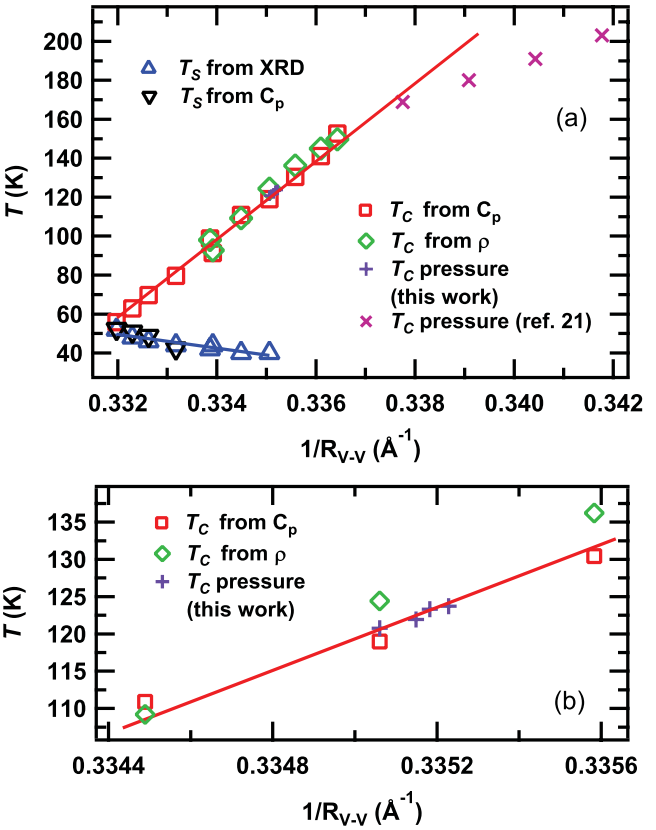

FIG. 12. (Color online) (a) Variation with $1/R_{V\text{-}V}$ of T_C and T_s for $Mn_{1-x}Co_xV_2O_4$. (b) Part (a) expanded in the range of $0.3344 \leqslant 1/R_{V\text{-}V} \leqslant 0.3356$ Å^{-1}.

when the system is pushed to the itinerant electron limit with increasing chemical pressure, the stronger electronic delocalization can lead to more dynamic homopolar V-V covalent bonds with fluctuating long and short V-V bonds, involving no obvious structural distortion and leaving $c/a \approx 1$. This trend for $Mn_{1-x}Co_xV_2O_4$ is consistent with our reported studies that there is no structural distortion for pure CoV_2O_4.[21]

V. CONCLUSION

In summary, for $Mn_{1-x}Co_xV_2O_4$, with increasing Co doping, the increasing chemical pressure (i) enhances the ferrimagnetic transition; (ii) suppresses the structural distortion; and (iii) drives the system toward to the itinerant electron limit by shrinking the V-V distance. The effects on AV_2O_4 of chemical pressure are similar to the effects of physical pressure, confirming that the V-V distance is a critical parameter controlling the structural, magnetic, and electronic behavior of AV_2O_4 spinels.

ACKNOWLEDGMENTS

This work is supported by NSF-DMR-0654118 and the State of Florida. A. Kiswandhi is supported in part by NSF-DMR 1005293.

*zhou@magnet.fsu.edu

[1] S.-H. Lee, H. Takagi, D. Louca, M. Matsuda, S. Ji, H. Ueda, Y. Ueda, T. Katsufuji, J.-H. Chung, S. Park, S.-W. Cheong, and C. Broholm, J. Phys. Soc. Jpn. **79**, 011004 (2010).

[2] M. Onoda and J. Hasegawa, J. Phys. Condens. Matter **15**, L95 (2003).

[3] G. Giovannetti, A. Stroppa, S. Picozzi, D. Baldomir, V. Pardo, S. Blanco-Canosa, F. Rivadulla, S. Jodlauk, D. Niermann, J. Rohrkamp, T. Lorenz, S. Streltsov, D. I. Khomskii, and J. Hemberger, Phys. Rev. B **83**, 060402(R) (2011).

[4] A. N. Vasiliev, M. M. Markina, M. Isobe, and Y. Ueda, J. Magn. Magn. Mater. **300**, e375 (2006).

[5] K. Adachi, T. Suzuki, K. Kato, K. Osaka, M. Takata, and T. Katsufuji, Phys. Rev. Lett. **95**, 197202 (2005).

[6] S.-H. Baek, N. J. Curro, K.-Y. Choi, A. P. Reyes, P. L. Kuhns, H. D. Zhou, and C. R. Wiebe, Phys. Rev. B **80**, 140406(R) (2009).

[7] K. Myung-Whun, J. S. Kim, T. Katsufuji, and R. K. Kremer, Phys. Rev. B **83**, 024403 (2011).

[8] K. Takubo, R. Kubota, T. Suzuki, T. Kanzaki, S. Miyahara, N. Furukawa, and T. Katsufuji, Phys. Rev. B **84**, 094406 (2011).

[9] V. O. Garlea, R. Jin, D. Mandrus, B. Roessli, Q. Huang, M. Miller, A. J. Schultz, and S. E. Nagler, Phys. Rev. Lett. **100**, 066404 (2008).

[10] M. Tanaka, T. Tokoro, and Y. Aiyama, J. Phys. Soc. Jpn. **21**, 262 (1996).

[11] T. Katsufuji, T. Suzuki, H. Takei, M. Shingu, K. Kato, K. Osaka, M. Takata, H. Sagayama, and T. Arima, J. Phys. Soc. Jpn. **77**, 053708 (2008).

[12] H. Mamiya, M. Onoda, T. Furubayashi, J. Tang, and I. Nakatani, J. Appl. Phys. **81**, 5289 (1997).

[13] E. M. Wheeler, B. Lake, A. T. M. N. Islam, M. Reehuis, P. Steffens, T. Guidi, and A. H. Hill, Phys. Rev. B **82**, 140406(R) (2010).

[14] M. Reehuis, A. Krimmel, N. Büttgen, A. Loidl, and A. Prokofiev, Eur. Phys. J. B **35**, 311 (2003).

[15] S.-H. Lee, D. Louca, H. Ueda, S. Park, T. J. Sato, M. Isobe, Y. Ueda, S. Rosenkranz, P. Zschack, J. Íñiguez, Y. Qiu, and R. Osborn, Phys. Rev. Lett. **93**, 156407 (2004).

[16] D. B. Rogers, R. J. Arnott, A. Wold, and J. B. Goodenough, J. Phys. Chem. Solids **24**, 347 (1963).

[17] D. B. Rogers, J. B. Goodenough, and A. Wold, J. Appl. Phys. **35**, 1069 (1964).

[18] J. B. Goodenough, in *Metallic Oxides*, edited by H. Reiss, Progress in Solid State Chemistry Vol. 5 (Pergamon, New York, 1972).

[19] S. Blanco-Canosa, F. Rivadulla, V. Pardo, D. Baldomir, J. -S. Zhou, M. García-Hernández, M. A. López-Quintela, J. Rivas, and J. B. Goodenough, Phys. Rev. Lett. **99**, 187201 (2007).

[20] V. Pardo, S. Blanco-Canosa, F. Rivadulla, D. I. Khomskii, D. Baldomir, Hua Wu, and J. Rivas, Phys. Rev. Lett. **101**, 256403 (2008).

[21] A. Kismarahardja, J. S. Brooks, A. Kiswandhi, K. Matsubayashi, R. Yamanaka, Y. Uwatoko, J. Whalen, T. Siegrist, and H. D. Zhou, Phys. Rev. Lett. **106**, 056602 (2011).

[22] K. Ståhl, [http://www.xray.kemi.dtu.dk/English/Computer%20Programs/WINPREP.aspx], Lyngby, Denmark.

[23] H. D. Zhou, J. Lu, and C. R. Wiebe, Phys. Rev. B **76**, 174403 (2007).

[24] N. F. Mott and E. A. Davis *Electronic Processes in Noncrystalline Materials* (Clarendon, Oxford, 1979).

[25] A. P. Ramirez, R. J. Cava, and J. Krajewski, Nature (London) **386**, 156 (1997).

[26] Z. Yang, S. Tan, and Y. Zhang, Phys. Rev. B **64**, 024401 (2001).

[27] Z. Yang, X. Bao, S. Tan, and Y. Zhang, Phys. Rev. B **69**, 144407 (2004).

[28] P. W. Anderson, Phys. Rev. **115**, 2 (1959).

[29] D. G. Wickham and J. B. Goodenough, Phys. Rev. **115**, 1156 (1959).